Geophysical Journal International

Geophys. J. Int. (2017) **210,** 390–405
Advance Access publication 2017 April 24
GJI Geomagnetism, rock magnetism and palaeomagnetism

doi: 10.1093/gji/ggx157

High-resolution mineralogical and rock magnetic study of ferromagnetic phases in metabasites from Oscar II Land, Western Spitsbergen—towards reliable model linking mineralogical and palaeomagnetic data

Mariusz Burzyński,[1] Krzysztof Michalski,[1] Krzysztof Nejbert,[2] Justyna Domańska-Siuda[2] and Geoffrey Manby[3]

[1]*Instytut Geofizyki PAN Księcia Janusza* 64, 01–452 *Warszawa, Poland. E-mail:* mburzynski@igf.edu.pl
[2]*Wydział Geologii, Uniwersytet Warszawski, al. Żwirki i Wigury* 93, 02–089 *Warszawa, Poland*
[3]*Natural History Museum of London, Great Britain, Cromwell Road, London, United Kingdom*

Accepted 2017 April 20. Received 2017 April 14; in original form 2016 September 29

SUMMARY

Typical 'whole rock' rock magnetic analyses are limited to the identification of the magnetic properties of the mixture of all ferromagnetic minerals within the samples. In this contribution standard 'whole rock' rock magnetic studies of two types of metabasites (metadolerites and metavolcanics) from the metamorphic Proterozoic–Lower Palaeozoic complex of Oscar II Land (Western Spitsbergen) are followed by separation of Fe-containing fractions and conducting magnetic analyses on Fe-containing separates. The main aim here is to determine if any ferromagnetic carriers of a palaeomagnetic signal preceding the Caledonian metamorphism persisted in the metabasites. A comprehensive set of applied methods has allowed for the precise identification of the ferromagnetic carriers and have revealed their textural context in the investigated rocks. The results of mineralogical and rock magnetic analyses of separates confirmed a dominance of low coercivity magnetite/maghemite and pyrrhotite in the metadolerites while in the metavolcanics the existence of magnetite/maghemite and hematite was highlighted. Our investigations support the hypothesis that Caledonian metamorphic remineralization has completely replaced the primary magmatic - Proterozoic/Lower Palaeozoic ferromagnetic minerals in the metadolerites. In the case of the metavolcanics, however, the existence of the ferromagnetic pre-Caledonian relicts cannot be excluded. Furthermore, this approach provided a unique opportunity for conducting rock magnetic experiments on natural mono-ferromagnetic fractions. The described methodologies and results of this study form a new approach that can be applied in further palaeomagnetic and petrographic studies of metamorphosed rock complexes of Svalbard.

Key words: Arctic region; Magnetic mineralogy and petrology; Palaeomagnetism applied to geologic processes; Rock and mineral magnetism.

1 INTRODUCTION

A critical point of any palaeomagnetic study is the identification of the origin of the palaeomagnetic signal carriers. Detailed mineralogical identification via scanning electron microscope (SEM), backscattered electron (BSE) imagery has enabled the differentiation and identification of particular ferromagnetic mineral associations that were generated during primary and subsequent tectonothermal events. In contrast, standard rock magnetic experiments usually offer only 'whole rock' analyses, during which the mean 'whole sample' signal is measured. In the latter, because of the large size of the samples, assignment of magnetic properties to particular generations of ferromagnetic minerals is usually impossible. Additionally, overlapping unblocking temperatures and coercivity spectra make ferromagnetic mineral identification difficult and ambiguous.

This contribution is focused on detailed rock magnetic investigations of two types of pre-Caledonian metabasic rocks located in the Proterozoic-Lower Palaeozoic metamorphic complex of Oscar II Land which forms part of the so called Western Svalbard Caledonian Terrane (Harland & Wright 1979; Harland 1997). The first type are metadolerites sheets from the vicinity of St. Jonsfjorden and Kinnefjellet, the second are metavolcanics of the Venernbreen moraine from the vicinity of Farmhamna (Fig. 1), that are represented by porous and massive rocks forming structures resembling pillow lavas. Both types of metabasites were subjected to greenschist

© The Authors 2017. Published by Oxford University Press on behalf of The Royal Astronomical Society.

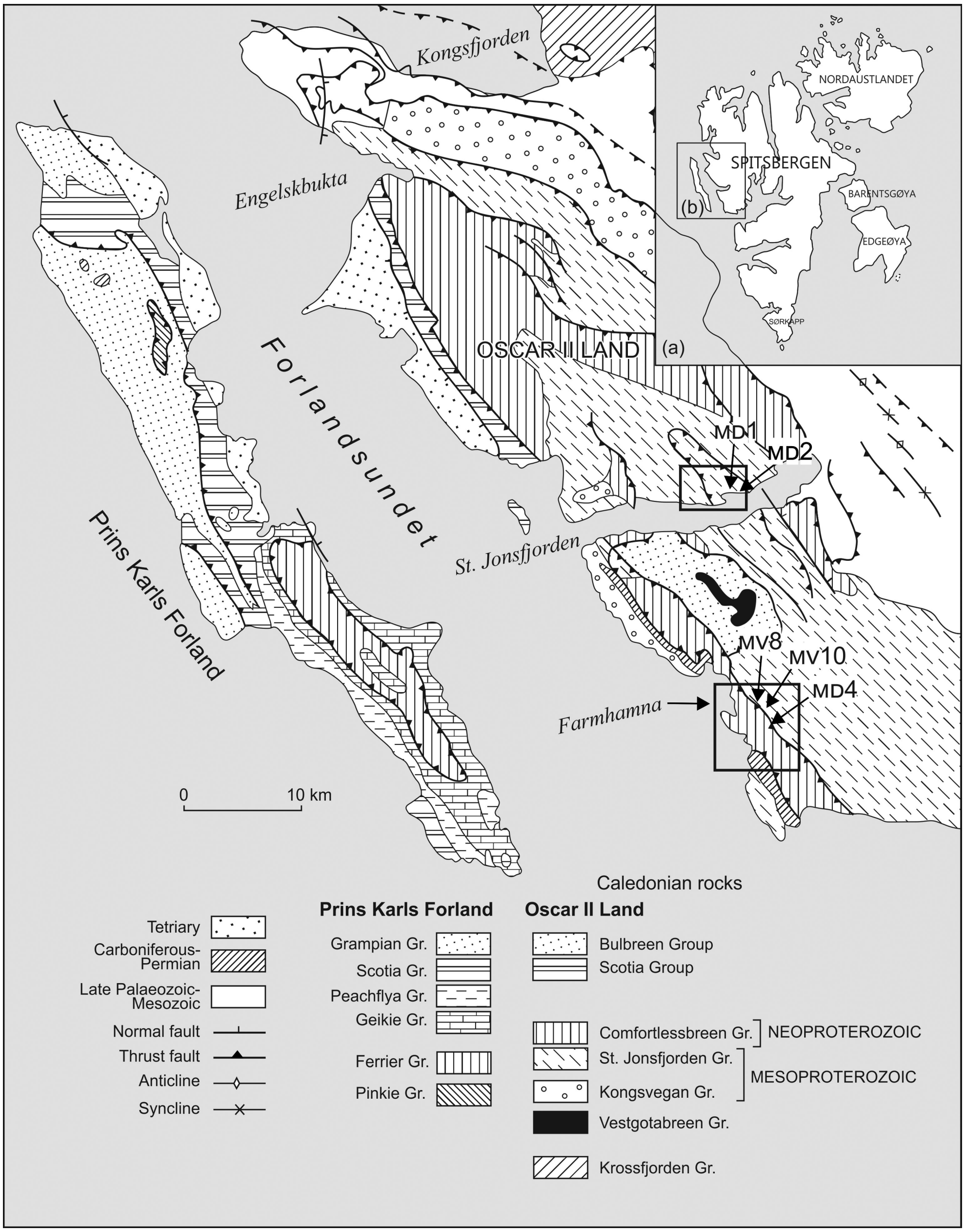

Figure 1. (a) Simplified contour map of Svalbard; square marks area of investigation. (b) Simplified geological map of Forlandsundet/Oscar II Land area; sampling sites are marked by squares and arrows; MD1-, MD2-metadolerites from St. Jonsfjorden, MD4-metadolerites from Kinnefjellet, MV8-, MV10-metavolcanics sites from Farmhamna (Venernbreen morain); symbols correspond to palaeomagnetic sites in Michalski *et al*. (2017).

facies Silurian/Devonian Caledonian metamorphism (e.g. Harland & Wright 1979; Ohta 1985; Hjelle *et al*. 1999) which constitutes the upper age limit of the investigated rocks. In the target area several post-Caledonian tectono-thermal episodes, which could have influenced the magnetic record and potentially generate new ferromagnetic minerals associations, also occurred. These events include a Late Devonian to Early Carboniferous Svalbardian Phase, Mesozoic rifting events, and the Late Cretaceous/Palaeogene Greenland-Svalbard convergence (Dallmeyer 1989; Tessensohn *et al*. 2001; Gasser & Andresen 2013; Clark *et al*. 2014).

The palaeomagnetism of Caledonian metamorphic complexes of Svalbard has been the subject of several publications (Maloof *et al*. 2006; Michalski *et al*. 2012, 2014). A detailed description of the palaeomagnetic properties of the investigated metabasites has been presented in a simultaneously submitted sister paper (Michalski *et al*. 2017). The latter contribution also presents new *in situ* laser ablation inductively coupled plasma mass spectrometry (LA-ICP-MS) 40Ar/39Ar age determinations of the adjacent rocks which provides evidence of the occurrence of three thermal events, which could have influenced the palaeomagnetic record of the metabasites in the 426–380 Ma, 377–326 Ma and *c*. 300 Ma intervals. The present investigations have revealed a complex natural remanent magnetization (NRM) structure of the metabasites, with often overlapping unblocking temperatures spectra of particular components (*cf.* Michalski *et al*. 2017). The main difficulty in defining the origin of the most stable characteristic remanent magnetizations (ChRMs) arises from the fact that their Virtual Geomagnetic Poles (VGPs) do not fall into any sector of Laurussia reference apparent polar wander path (APWP). Consequently, palaeomagnetic components cannot be directly dated by the palaeomagnetic method.

Table 1. A summary of the petrographic and rock magnetic methods.

	Petrographic methods		Rock magnetic methods		
Samples	Optical microscopy	SEM/BSE	Hysteresis parameters	SIRM	Lowrie test
Whole rock	+	+	+	+	+
Separates	+	+	+	+	–

There are several palaeogeographic (great circle/small circle models) and regional tectonic models (normal thrusting/listric faulting models) which can be applied to explain the inconsistency of the observed directions with the reference path (Michalski *et al*. 2017). In applying any of these models a substantial question arises as to the age of the remagnetization. If direct isotopic age determinations of the target rocks are not available, then detailed petrographic and structural observations of the ferromagnetic carriers defining their geometrical relations to other mineral associations forming the metabasites become crucial. In this particular case, the first step to discover the origin of the NRM is answering the question as to whether there any relicts of pre-Caledonian greenschist facies metamorphism directions preserved in the investigated rocks.

In this study several procedures were applied to describe and better understand the magnetic properties of the coexisting ferromagnetic mineral associations in the metabasites. Initially, examinations of the thin sections (optical/SEM/BSE) were conducted. These were supported by standard 'whole rock' magnetic analyses including coercivity spectra measurements using Vibrating Sample Magnetometer (VSM), saturation isothermal remanent magnetization (SIRM) measurements and three-component isothermal remanent magnetization (IRM) procedures (Lowrie 1990). All of the 'Fe-containing' associations identified during the microscopic observations of the samples were then separated. Each of the magnetic fractions were again subjected to rock magnetic (SIRM/Micromag and VSM) and mineralogical (optical/SEM/BSE) investigations. Similar experiments conducted on 'Fe-containing' fractions have been described in the literature (e.g. Dekkers 1988; Dunlop *et al*., 2005, 2006) but were rarely performed on natural rock samples and have never been applied to metamorphic and magmatic rocks of Spitsbergen. Finally, assessments of the procedures employed to identify the ferromagnetic carriers as well as the degree to which these may have helped in determining the origin of metabasites NRMs are attempted.

2 MATERIALS AND METHODS

2.1 Petrographic and mineralogical methods

Petrographic and mineralogical investigations were carried out at the Inter-Institute Analytical Complex, Faculty of Geology, University of Warsaw. The identification of the mineral assemblages was conducted using a NIKON ECLIPSE E600 POL microscope. The compositions of the ferromagnetic minerals and BSE images were determined using a CAMECA SX 100 electron microprobe equipped with wavelength-dispersive spectrometers (15 kV and 20 nA, PAP correction procedure). During the investigations natural and synthetic standards supplied by SPI and CAMECA were used.

2.2 Ferromagnetic minerals separation

Five palaeomagnetic samples (1–2 kg each of them) representing both investigated lithologies (three from the metadolerites and two from the metavolcanics) from five palaeomagnetic sites (Fig. 1b) were chosen for ferromagnetic minerals separation. The main purpose of this step was to separate the main magnetic carriers identified in the course of the optical microscopy investigations.

All samples were crushed, ground and sieved in the laboratory at the Faculty of Geology, University of Warsaw using a Testchem LKS-60 crusher and a Testchem LMŻ grinder. The minerals were then divided into 0.6 mm > Ø > 0.4 mm, 0.4 mm > Ø > 0.2 mm, 0.2 mm > Ø > 0.1 mm, Ø < 0.1 mm size groups. The magnetic residuum was then separated from non-magnetic phases using a hand neodymium magnet (REE Tube Magnet, Eriez Magnetics Europe Limited). After the preliminary coercivity spectra research, conducted on the MicroMag magnetometer, the 0.4 mm > Ø > 0.2 mm size range was chosen as most suitable for further investigation. The Ø < 0.2 mm groups did not have a sufficiently strong enough magnetic signal to be recorded using the MicroMag magnetometer. Grains larger than Ø > 0.4 mm appeared to be multi-mineral aggregates and this group was also excluded from further investigations.

Finally, seven different groups of grains in the size range 0.4 mm > Ø > 0.2 mm were distinguished (five from the metadolerites and two from the metavolcanics) using a stereoscopic microscope. Six of the grain groups were found to possess a useful ferromagnetic signal while one group of Fe-containing grains separated from the metadolerites revealed a paramagnetic hysteresis loop.

All petrographic and rock magnetic methods conducted on 'whole rock' samples and separates are summarized in Table 1.

2.3 Rock magnetic methods

All rock magnetic experiments were carried out at the Department of Laboratory of Palaeomagnetism, Institute of Geophysics, Polish Academy of Sciences.

The parameters of the hysteresis loops (M_s–saturation magnetization; M_{rs}–saturation remanence; B_c–coercivity field; B_{cr}–coercivity of remanence) of the 'whole rock' samples were determined using a Molspin Ltd, UK vibrating magnetometer VSM in maximum field 1 T. Within the separates hysteresis loop experiments were performed using a PMC MicroMag 2900 Series AGM VSM. As the MicroMag magnetometer can measure fine grained material (particles below 0.2 mm), it was used at first to determine whether the separates exhibited any ferromagnetic signal before qualifying them for further analyses.

The maximum unblocking temperatures ($T_{ub\ max}$) were estimated based on the SIRM decay curves (Kądziałko-Hofmokl & Kruczyk 1976), both for 'whole rock' samples, as well as for monoferromagnetic loose separates. In the case of loose material, to proceed the SIRM experiment it was necessary to put the samples into aluminium foil. In cases where the amount of separated ferromagnetic grains was low a quartz powder was used as a cement. The samples were magnetized in a 7 T field using a MMPM–10 (magnetic measurements pulse magnetizer) and after that heated twice using the furnace coupled with a spinner magnetometer up to 700 °C in a field-free space. The first demagnetization curve showed $T_{ub\ max}$ characteristic for particular ferromagnetic phases existing in

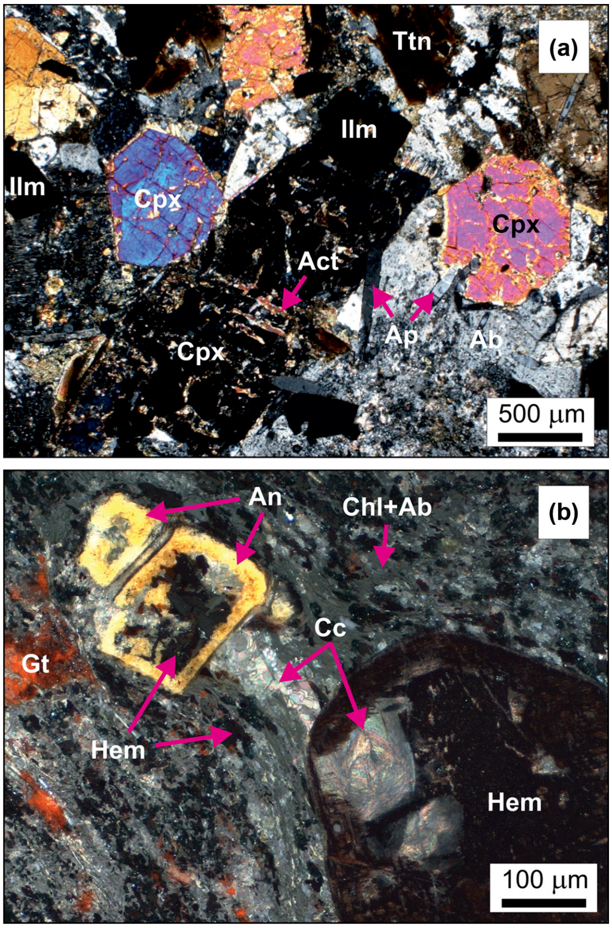

Figure 2. Petrography of the metadolerites and metavolcanites. (a) Metadolerite with well-preserved primary magmatic intersertal texture, St. Jonsfjorden, site MD1. (b) Metavolcanite with porphyritic texture containing large clasts of other volcanic rocks (see right-bottom part of the image), Farmhamna, site MV8; both photo-images were taken using transmitted polarized light under crossed Nicols. Abbreviations: Ab, albite; Act, actinolite; An, anatase; Ap, apatite; Bt, biotite; Cc, calcite; Chl, chlorite; Cpx, clinopyroxene; Gt, goethite; Hem, hematite; Ilm, ilmenite; Ttn, titanite.

the sample. On the second curve it was possible to observe $T_{\mathrm{ub\,max}}$ of ferromagnetic phases generated during first heating.

A more precise identification of unblocking temperatures of particular ferromagnetic grains differentiated by coercivity spectra was derived from the three-component IRM procedure (Lowrie 1990). In that experiment samples were magnetized in three perpendicular directions in different magnetic fields—0.12, 0.4, and 3 T, respectively—and then stepwise thermally demagnetized in a field-free magnetic furnace MMTD1 (Magnetic Measurements Thermal Demagnetiser of Great Britain). After each demagnetization step the residual magnetic remanence of the samples were measured on the Superconducting Quantum Interference Device (SQUID, 2 G Enterprise model 755, USA) with a residual internal field of below 3 nT and a noise level of about 5 μA m^{-1}. As the experiment required cylindrical cores, it was conducted only on 'whole rock' samples.

2.3.1 Palaeomagnetic procedures

Detailed description of the applied palaeomagnetic procedures as well as the presentation of the results of the palaeomagnetic investigations are the subject of companion paper (Michalski *et al.* 2017). The thermal stepwise demagnetization method up to 680 °C appeared to be the most effective in extracting the NRM components of the investigated metabasites. In the course of the thermal demagnetization 12 components, which passed the criteria: $\kappa >$ 10, $\alpha95\% < 16\,^{\circ}$, were identified and qualified for further tectonic and paleogeographic interpretation (Michalski *et al.* 2017, their fig. 9, tables 3 and 5). An alternating Field (AF) demagnetization was conducted as a supplementary procedure. Three samples from each of the sites were stepwise demagnetized up to 160 mT. Three other specimens from each of the sites were demagnetized in the AFs up to 20 mT and then subjected to regular thermal demagnetization. Unfortunately, none of the above experiments, neither pure AF, nor combined AF/thermal demagnetization experiments provided reliable results. In only few specimens was it possible to calculate the directions below 20 mT. In only one site did the results of AF demagnetization qualify for further tectonic interpretation; component MD6AFL (38.4/65.3; $\alpha95 = 15.5\,^{\circ}$, $\kappa = 19.75$; Michalski *et al.* 2017, their fig. 9, table 3).

3 'WHOLE ROCK' INVESTIGATIONS

3.1 Petrography of metadolerites

The metadolerites are medium- to coarse-grained and primary doleritic to gabbroic textures were well preserved in a number of the samples (e.g. in the St. Jonsfjorden metadolerite dyke; Fig. 2a). In this locality, only the marginal parts of the metadolerite bodies are schistose in texture (Ohta 1985). The textures of the metadolerites from Kinnefjellet vary among the samples with very well preserved magmatic textures to those that have been strongly dynamically recrystallized with well-defined metamorphic foliations. The groundmass mineral composition of the metadolerites is illustrated in Fig. 2(a).

The ferromagnetic phases in mafic rock are largely composed of the oxide and sulphide associations (Frost & Lindsley 1991; Haggerty 1991). In the metadolerites, the magmatic oxides are represented by ilmenite phenocrysts (Figs 3a–c). No microscopically visible relicts of unaltered magmatic magnetite in association with the Fe-Ti-oxides were identified but numerous titanite pseudomorphs after magmatic magnetite (Figs 3a & d, and 4a & b) were observed.

The sulphide aggregates consist of complex intergrowths of pyrite and pyrrhotite, however, monomineralic aggregates also occur (Figs 4a–d). Pyrite may also associate with chalcopyrite, sphalerite and galena. The large pyrite aggregates may include minute intergrowths of pyrrhotite and magnetite-like minerals (Figs 4a–c). Their optical features are close to that observed in the magnetite, while their chemical composition corresponds to maghemite or non-stoichiometric magnetite (Supporting Information Appendix A).

The following mineral associations have been classified as potential main magnetic carriers in metadolerites:

(1) Ilmenite phenocrysts (MD-Ilm). This group of grains, represented by magmatic ilmenites, revealed a possible existence of primary ferromagnetic intergrowths. The presence of small lens-like open spaces within the ilmenite phenocrysts (Fig. 3c) unequivocally documents an earlier presence of hematite exsolution intergrowths (compare Haggerty 1991).

(2) Titanite pseudomorphs after primary magnetite (MD-psMag). This group of grains was chosen to confirm the presence of sub-optical intergrowths of primary or secondary magnetite which

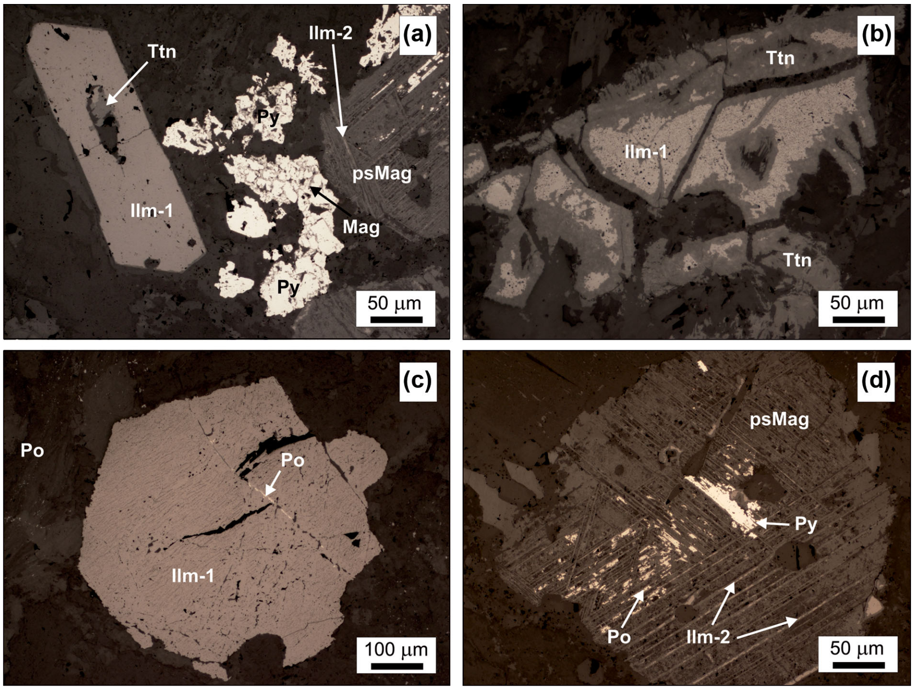

Figure 3. Fe-Ti oxides and their breakdown products recognized in the metadolerites. All photo-images were taken using reflected polarized light under parallel Nicols. (a) Oxide–sulphide association, developed during magmatic and metamorphic processes, represented by primary ilmenite (Ilm-1) and breakdown product of magmatic pyrrhotite and magnetite. The last phases are now represented by pyrite-magnetite and titanite-ilmenite (Ilm-2)-pyrite intergrowths, respectively. St. Jonsfjorden, site MD1. (b) Ilmenite grain replaced by titanite. St. Jonsfjorden, site MD2. (c) Ilmenite grain with metamorphic pyrrhotite veinlet. Grey pattern within entire grain are small lens-like open spaces after dissolved exsolutions of hematite. St. Jonsfjorden, site MD1. (d) Titanite pseudomorph after magmatic Ti-bearing magnetite. Within the pseudomorph are remnants of oxy-exsolved ilmenite (Ilm-2) and aggregates of metamorphic pyrrhotite and pyrite occur. St. Jonsfjorden, site MD1. Abbreviations: Ilm, ilmenite; Po, pyrrhotite; Py, pyrite; Ttn, titanite psMag, titanite pseudomorph after magnetite; Mag, magnetite.

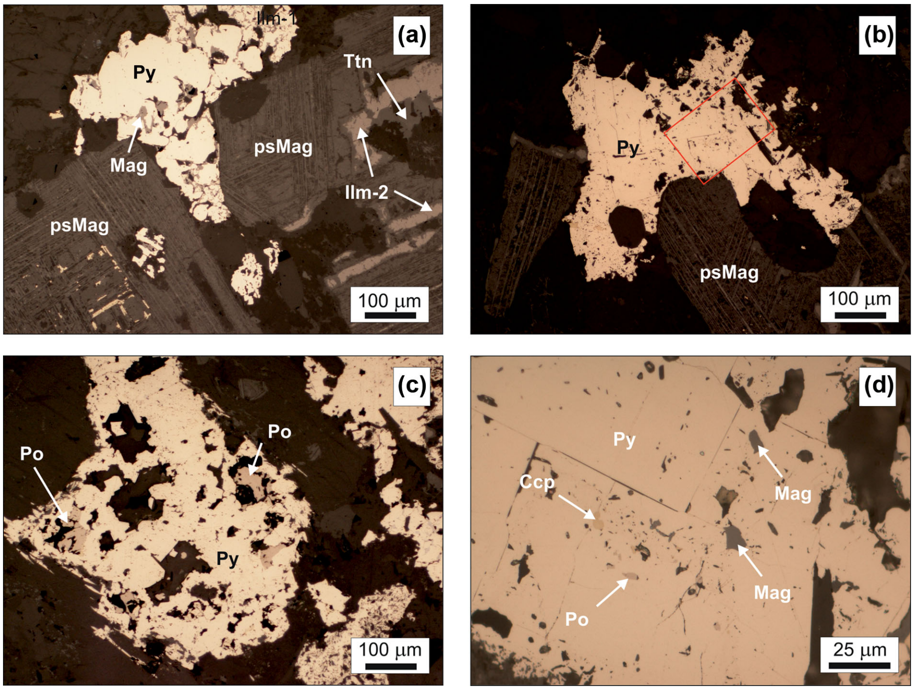

Figure 4. Sulphides with magnetite and/or pyrrhotite associations in metadolerites. All photo-images were taken using reflected polarized light under parallel Nicols. (a) Pyrite/magnetite intergrowths developed during pyrrhotite breakdown. Small amounts of both phases also form minute intergrowths within titanite pseudomorphs after magnetite, St. Jonsfjorden, site MD1. (b) Pyrite aggregate after primary magnetite. Details of inclusion mineralogy from area marked by red rectangle are presented on microphotograph D (this plate). St. Jonsfjorden, site MD1. (c) Metamorphic pyrite grain with pyrrhotite intergrowths. St. Jonsfjorden, site MD1. (d) Inclusions of magnetite/maghemite, pyrrhotite and chalcopyrite preserved in a large pyrite grain. St. Jonsfjorden, site MD1. Abbreviations: Ccp, chalcopyrite; Ilm, ilmenite; Mag, magnetite; Po, pyrrhotite; Py, pyrite; Ttn, titanite; psMag, titanite pseudomorph after magnetite.

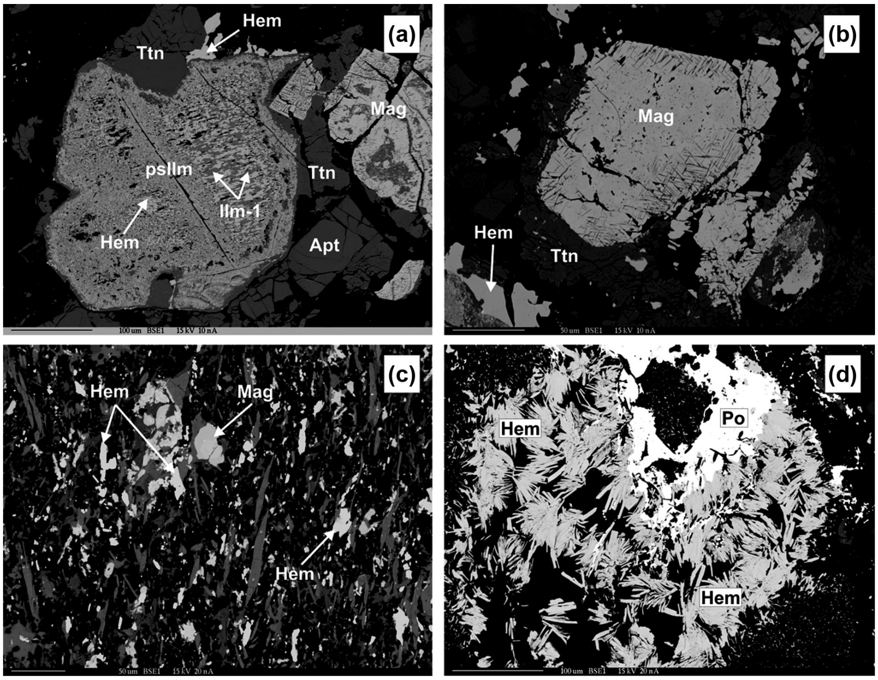

Figure 5. Fe-Ti-oxides associations recognized within metavolcanic rocks from Farmhamna (Venernbreen morain). All backskatter electron images (BSE) were taken using CAMECA SX100 microprobe. (a) Titanite and anatase pseudomorph after primary magmatic ilmenite and magnetite with relics of primary minerals, Farmhamna, site MV8. (b) Altered magnetite rimmed by metamorphic titanite. Farmhamna, site MV8. (c) Numerous grains of hematite and ilmenite within fine-grained matrix of metavolcanic rock. Farmhamna, site MV8. (d) Aggregates of metamorphic hematite and pyrrhotite. Farmhamna, site MV8. Abbreviations: Apt, apatite; Ilm, ilmenite; Mag, magnetite; Po, pyrrhotite; Ttn, titanite; psIlm, titanite and anatase pseudomorph after ilmenite; psMag, titanite pseudomorph after magnetite.

could survive as a result of the incomplete breakdown of magmatic magnetite into titanite or which crystalized contemporaneously with titanite during metamorphic events (Xirouchakis & Lindsley 1998; Harlov *et al*. 2006). These grains commonly contain remnants of oxy-exsolved ilmenite (Ilm-2) and rare sulphide intergrowths that grew significantly later (Fig. 3d).

(3) Pyrites (MD-Py). Represented by grains of metamorphic origin with numerous intergrowths of magnetite and sulphides such as chalcopyrites and pyrrhotites (Fig. 4d). Such intergrowths and textures of pyrite aggregates indicate that they all crystallized during greenschist metamorphism and are breakdown products of the earlier pyrrhotite (Ramdohr 1980). The minute magnetite intergrowths observed under polarized reflected light revealed typical magnetite features. Microprobe data (Supporting Information Appendix A) show, however, that nearly all of the iron occurs in the trivalent state in the structure of this oxide. These data suggest that magnetite-like intergrowths have structure similar to maghemite.

(4) Pyrrhotites (MD-Po). Which are dominant in the metadolerites from Kinnefjellet are mostly homogenous grains and represent metamorphic phases of the ferromagnetic minerals. In the unaltered pyrrhotites small exsolution lamellae of pentlandite intergrowths were observed.

3.2 Petrography of the metavolcanic rocks

The metavolcanic rocks are commonly porphyritic (Fig. 2b) and the altered phenocrysts often define melt flow textures. Some samples are clearly of pyroclastic origin and are characteristically heterogeneous in composition. The volcanic rocks were strongly overprinted during the Caledonian (*sensu lato*) greenschist facies metamorphism. The mineralogy of the fine-grained matrix of these rocks is microscopically difficult to identify. Their mineralogical composition is presented in Figs 2(b) and 5. The massive textured metavolcanics are characterized by the presence of amphibole and biotite phenocrysts (commonly replaced by chlorite aggregates) and subordinate minor feldspar crystals (Fig. 2b). In the studied rocks irregular, calcite filled, lenses are common. Quartz–calcite aggregates that resemble pseudomorphs after plagioclase also occur. The partially altered magnetite and ilmenite phenocrysts (Figs 5a and b), surrounded by titanite and low-temperature Ti-oxides were observed.

The ferromagnetic phases are dominated by magnetite and hematite. They are represented mostly by metamorphic assemblages as indicated by their euhedral habits and intergrowths with metamorphic albite–chlorite–actinolite. Textural relationships (Supporting Information Appendix B) suggest their nearly contemporaneous growth during greenschist facies metamorphism, with an oxygen fugacity (fO2) that can be constrained to *ca.* −30 log units (Dalstra & Guedes 2004; Hurai & Huraiová 2011). The primary magmatic Fe-Ti oxides occur only as relict phenocrysts up to 0.5 mm (Figs 2b, and 5a and b), strongly replaced by titanite and anatase. (Figs 5b and c). The pyrrhotite and pyrite constitute subordinate components of the metavolcanic rocks (Fig. 5d).

The following mineral associations have been classified as the potential main magnetic carriers of metavolcanic rocks:

(1) Magnetite (MV-amf, MV-WR)—represented by minor magmatic and major metamorphic phases occurring as intergrowths in amphibolites and dispersed in the matrix (Figs 5b and c).

(2) Hematite (MV-WR)—mostly belongs to metamorphic stages that crystalized as tabular grains in the matrix (Figs 5b and c).

Additional microscopic images of the investigated metadolerites and metavolcanics are presented in Supporting Information Appendix B.

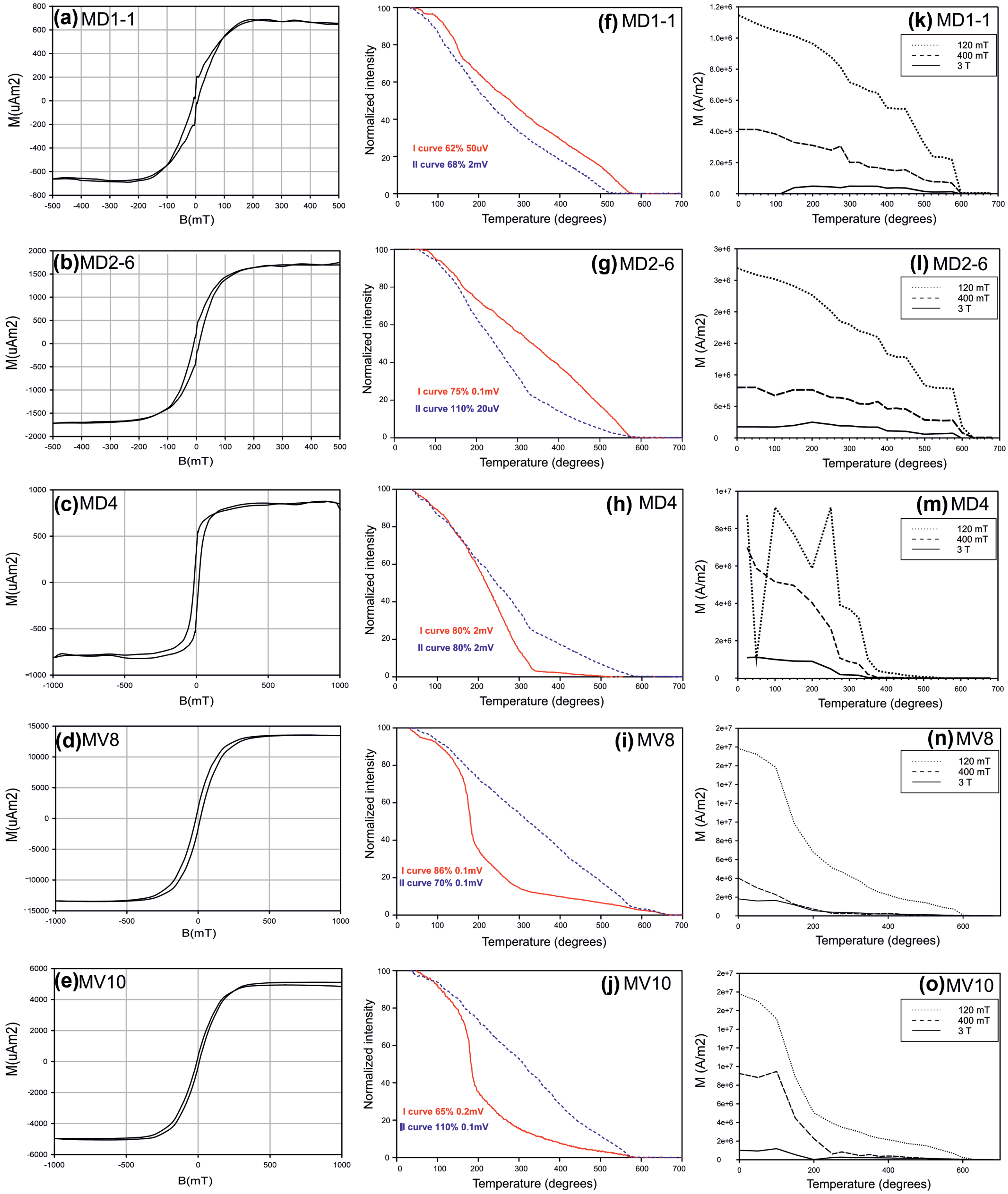

Figure 6. 'Whole rock' rock magnetic studies of investigated metabasites: (a–e) Hysteresis loops obtained in the course of VSM experiments; (f–j) SIRM experiments (solid line, first heating curve; dashed line, second heating curve); (k–o) three-component IRM experiments (dotted line, ferromagnetic fraction saturated up to 120 mT; dashed line, ferromagnetic fraction saturated up to 400 mT; solid line, ferromagnetic fraction saturated up to 3 T); metadolerites: MD1-1, MD2-6, MD4; metavolcanics: MV8, MV10.

3.3 'Whole rock' rock magnetic experiments

Hysteresis loops for all of the investigated 'whole rock' samples exhibit a ferromagnetic character (Fig. 6, left column). Parameters of magnetic hysteresis were presented in Table 2. They indicate the existence of low-coercivity phases in the metadolerites and low-middle coercivity minerals in the metavolcanics accordingly. The M_{rs}/M_s and B_{cr}/B_c ratios were plotted on Day-Dunlop diagram (Dunlop 2002, fig. 9). Most of the samples fall into

Table 2. Hysteresis parameters (M_s, M_r, B_c, B_{cr}), magnetic ratio (M_r/M_s), and coercivity ratio (B_{cr}/B_c). 1-8-'whole rock' metadolerite samples; 9-11-'whole rock' metavolcanic samples; 12-28- metadolerite separates; 29-41-metavolcanic separates.

No.	Samples categories	Description	M_s (A m^2)	M_r (A m^2)	B_c (mT)	B_{cr} (mT)	M_r/M_s	B_{cr}/B_c
1	MD1-1	'whole rock'-metadolerites	3.58E-06	4.80E-07	7.000	40.000	0.134	5.714
2	MD1-2		9.17E-06	1.41E-06	9.000	35.000	0.154	3.889
3	MD2-3		8.06E-06	1.81E-06	7.000	22.500	0.225	3.214
4	MD4-1		1.10E-05	3.40E-06	17.000	37.000	0.309	2.176
5	MD4-2		1.04E-06	1.00E-07	2.000	48.000	0.096	24.000
6	MD4-3		4.84E-05	1.84E-05	16.500	23.000	0.381	1.394
7	MD4-4		4.35E-06	7.90E-07	11.000	50.000	0.182	4.545
8	MD4-5		1.92E-05	4.90E-06	9.500	25.000	0.255	2.632
9	MV8-1	'whole rock'-metavolcanics	1.03E-03	1.00E-04	10.500	95.000	0.097	9.048
10	MV8-2		8.00E-04	8.66E-05	15.000	76.000	0.108	5.067
11	MV10		2.65E-03	1.75E-04	8.500	66.000	0.066	7.765
12	MD-Po	metadolerite- pyrrhotite 1	7.33E-07	2.49E-07	8.410	9.786	0.339	1.164
13		metadolerite-pyrrhotite 2	1.52E-07	4.99E-08	6.659	9.620	0.328	1.445
14		metadolerite-pyrrhotite 3	2.78E-07	9.00E-08	4.984	6.761	0.324	1.357
15		metadolerite-pyrrhotite 4	5.72E-07	2.01E-07	6.641	7.331	0.352	1.104
16		metadolerite-pyrrhotite 5	1.87E-07	7.44E-08	12.200	13.960	0.398	1.144
17	MD-Py	metadolerite-pyrite 1	1.16E-07	1.37E-08	6.814	14.350	0.118	2.106
18		metadolerite-pyrite 2	2.61E-07	3.82E-08	6.643	13.200	0.146	1.987
19	MD-psMag	metadolerite-titanite pseudomorphs after magnetite 1	6.76E-09	2.36E-09	14.390	27.820	0.349	1.933
20		metadolerite-titanite pseudomorphs after magnetite 2	3.10E-09	3.54E-10	9.985	29.610	0.114	2.965
21		metadolerite-titanite pseudomorphs after magnetite 3	1.31E-08	4.71E-09	9.464	18.960	0.360	2.003
22		metadolerite-titanite pseudomorphs after magnetite 4	8.60E-08	1.94E-08	7.521	22.220	0.225	2.954
23		metadolerite-titanite pseudomorphs after magnetite 5	4.95E-08	1.88E-08	13.890	24.860	0.380	1.790
24	MD-oxPy	metadolerite-oxidized sulphides 1	9.01E-06	1.44E-07	2.875	17.240	0.016	5.997
25		metadolerite-oxidized sulphides 2	8.24E-06	2.52E-07	2.688	13.220	0.031	4.918
26		metadolerite-oxidized sulphides 3	4.75E-06	7.87E-08	1.341	10.480	0.017	7.815
27		metadolerite-oxidized sulphides 4	5.92E-06	1.01E-07	2.141	13.640	0.017	6.371
28		metadolerite-oxidized sulphides 5	2.24E-06	1.09E-07	3.890	15.600	0.048	4.010
29	MV-WR	metavolcanic-grains with hematite and magnetite 1	1.91E-07	1.83E-08	11.170	91.500	0.096	8.192
30		metavolcanic-grains with hematite and magnetite 2	1.24E-07	1.29E-08	12.380	95.370	0.104	7.704
31		metavolcanic-grains with hematite and magnetite 3	2.09E-07	1.69E-08	8.503	83.340	0.081	9.801
32		metavolcanic-grains with hematite and magnetite 4	2.09E-07	1.35E-08	7.489	89.970	0.065	12.014
33		metavolcanic-grains with hematite and magnetite 5	3.41E-07	5.56E-08	20.420	106.100	0.163	5.196
34		metavolcanic-grains with hematite and magnetite 6	5.51E-07	6.48E-08	12.620	84.550	0.118	6.700
35		metavolcanic-grains with hematite and magnetite 7	4.76E-07	7.52E-08	19.250	101.200	0.158	5.257
36		metavolcanic-grains with hematite and magnetite 8	3.95E-07	5.35E-08	17.330	103.900	0.136	5.995
37	MV-Amf	metavolcanic-amphiboles with magnetite 1	1.49E-07	1.47E-08	8.222	40.160	0.099	4.884
38		metavolcanic-amphiboles with magnetite 2	9.89E-08	7.70E-09	8.971	63.730	0.078	7.104
39		metavolcanic-amphiboles with magnetite 3	4.51E-08	5.43E-09	10.510	45.110	0.120	4.292
40		metavolcanic-amphiboles with magnetite 4	8.33E-08	8.39E-09	10.380	70.400	0.101	6.782
41		metavolcanic-amphiboles with magnetite 5	1.39E-07	2.81E-08	23.560	100.200	0.202	4.253

a pseudo-single domain area revealing linear distribution shape. Only one metadolerite sample MD4 is located on single domain reference curve.

SIRM decay curves for the metadolerite sample MD4 from Kinnefjellet shows a decrease of magnetization up to 330 °C which is interpreted as $T_{\mathrm{ub\,max}}$ of pyrrhotite (Fig. 6f). The same sample also contains a small amount of low-Ti magnetite/maghemite with $T_{\mathrm{ub\,max}}$ near 530 °C. The SIRM first heating curves for the following two metadolerites samples from St. Jonsfjorden MD1-1, MD2-6 gently slope up to temperature 580 °C which indicates the presence of magnetite (Figs 6g and h). In all three metadolerite samples a significant increase of intensity of magnetization after first heating is observed due to the appearance of new magnetic minerals during conducted SIRM experiments (mainly magnetite and pyrrhotite). For metavolcanic samples (MV8, MV10) both SIRM curves reveal a major decrease of magnetic intensity (by 60–70 per cent of initial intensity) already in temperature range 150–200 °C. Both samples demagnetize completely by temperatures 580 and 680 °C, indicating the existence of magnetite and hematite respectively (Figs 6i and j). In contrast to the metadolerites, the metavolcanics do not reveal a significant increase of magnetization after first heating. On second heating, however, the characteristic 150–200 °C temperature SIRM curves are no longer observed.

More detailed characteristics of $T_{\mathrm{ub\,max}}$ related to particular coercivity fractions were obtained from three component IRM procedures described by Lowrie (1990). In the metadolerites the Lowrie test confirmed the dominance of low coercivity fractions and the existence of pyrrhotite in sample MD4 (Kinnefjellet) demagnetized up to 350 °C (Fig. 6k). Samples MD1-1, MD2-6 (St. Jonsfjorden), however, revealed temperatures around 600–630 °C which are higher than the SIRM maximum that are characteristic for the $T_{\mathrm{ub\,max}}$ of maghemite. Surprisingly in the case of metavolcanics, characteristic 150–200 °C temperatures were observed only on low-middle coercivity curves (Figs 6n and o) excluding the existence of high coercivity goethite ($T_{\mathrm{ub\,max}}$ = 120 °C; Dunlop & Özdemir 1997).

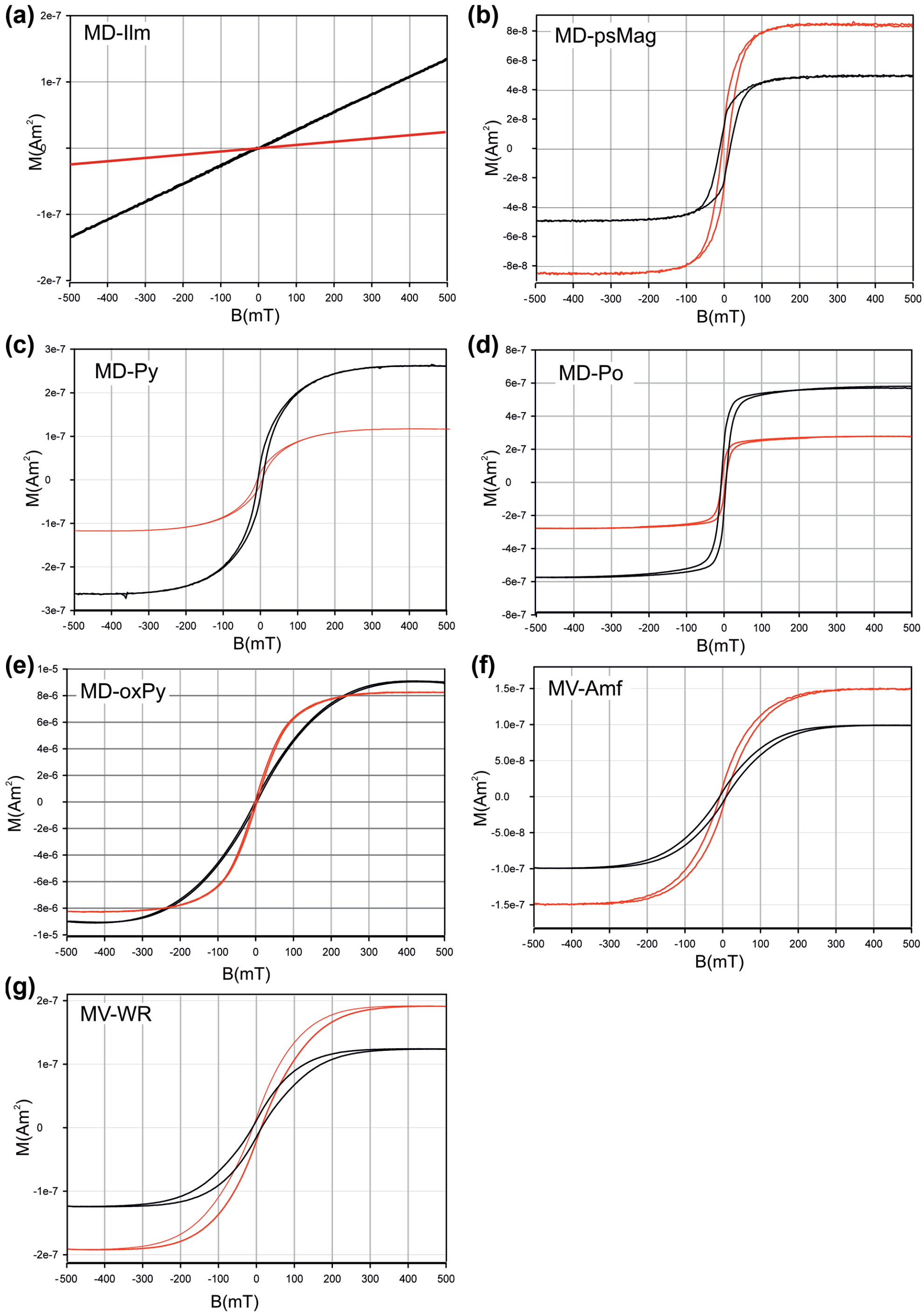

Figure 7. Examples of magnetic hysteresis loops of metadolerites (a–e) and metavolcanics (f–g) separates. Black colour, first sample; red colour, second sample.

It can be argued that a decrease of magnetization around 200 °C of the metavolcanics can be related to demagnetization of small grains of magnetite/maghemite with lower $T_{\mathrm{ub\,max}}$ (Özdemir 1987; Matzka & Krasa 2007). Similar low $T_{\mathrm{ub\,max}}$ temperatures were observed in maghemite rings on magnetite grains formed during low temperature oxidation (Kądziałko-Hofmokl 2001). The higher 600–620 °C temperatures observed on the low-coercivity Lowrie curves for the metavolcanics (Figs 6n and o) may indicate the presence of maghemite.

4 ANALYSES OF THE FERROMAGNETIC SEPARATES

The nomenclature and description of the seven different groups of grains (five from metadolerites and two from metavolcanics) that were distinguished from the Fe-containing fraction in the process of separation are summarized in Table 2.

The MicroMag magnetometer analyses proved that six of seven distinguished groups possessed hysteresis loops with the shapes and parameters of ferromagnetic minerals (Fig. 7). Group MD-Ilm

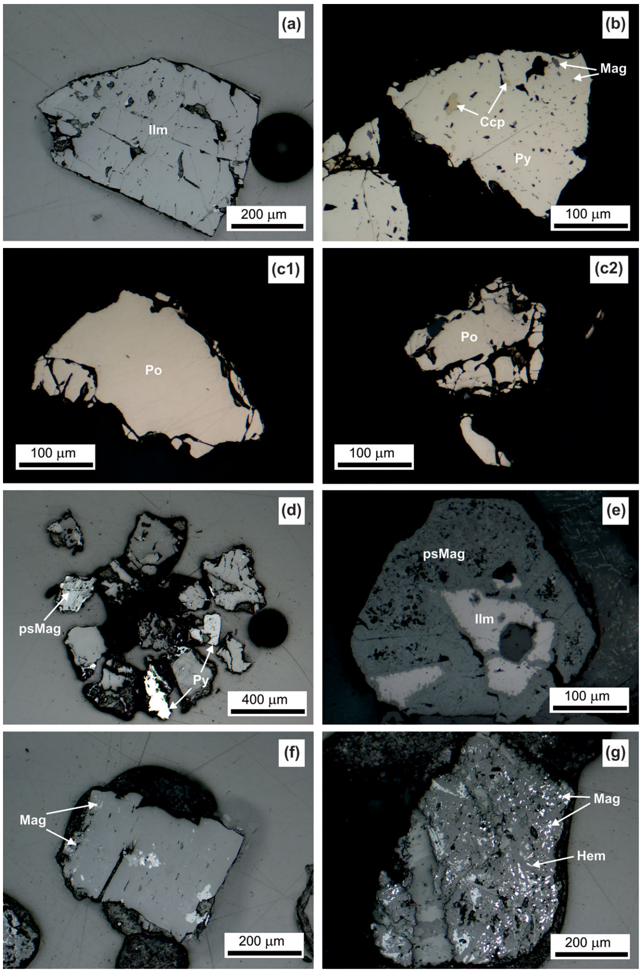

Figure 8. Photo-images of 'Fe-containing' separates from metabasites (Oscar II Land). Polarizing microscope, reflected light, one polar. (a) Fragment of the ilmenite phenocryst from metadolerite at St. Jonsfjorden, sample MD-Ilm. (b) Pyrite grains with numerous chalcopyrite and magnetite inclusions, MD-Py; (c1), (c2)—fragments of unaltered pyrrhotite aggregates, MD-Po. d) Metadolerite fragments cemented by oxidized sufphides, MD-oxPy. (e) Titanite pseudomorphs after magmatic magnetite. Irregular ilmenite intergrowths (Ilm-1, see Fig. 4a) developed due to oxy-exsolution processes, MD- psMag. (f) Amphibole grain with numerous small blebs of magnetite, MV- Amf. (g) Fragment of fine-grained metavolcanic matrix with numerous small grains of magnetite and hematite (white small grains), MV-WR.

appeared to be paramagnetic and was excluded from further rock magnetic investigations (however optical/SEM images of MD-Ilm were presented).

4.1 Mineralogy of the separates

4.1.1 Metadolerites

(1) The group MD-Ilm- represents the monomineralic grains of ilmenite with an average size of 400 μm (Fig. 8a). This group of ilmenite separates corresponds to the ilmenite phenocrysts preserved in a partially recrystallized metadolerite (compare Figs 3a–c). The chemical compositions of the ilmenite phenocrysts are presented in Supporting Information Appendix A.

(2) The group MD-psMag consists of titanite pseudomorphs after primary/magmatic magnetite where the grain sizes range from 300 to 400 μm in diameter. This group of separates corresponds to the common titanite pseudomorph after phenocrysts of magnetite observed in un-recrystallized dolerite samples, and illustrated on Figs 3(d) and 4(a). Optical, SEM+EDS and EPMA observations do not confirm the presence of magmatic magnetite in this grain category.

(3) The group MD-Py contains particles of pyrite that range in size from 200 to 400 μm in diameter (Fig. 8b). The chemical composition of the examined pyrite is nearly stoichiometric (Supporting Information Appendix A). This type of separates correspond well with abundant pyrite aggregates common in all of the metadolerite samples and given in Figs 4(a)–(c).

(4) The group MD-Po is represented by pyrrhotite grains, which are dominant in the Kinnefjellet metadolerites, have an average size 200 μm in diameter. Most of the grains are homogenous without any intergrowths (Fig. 8c1). A few separated pyrrhotites show partial alteration to marcasite during which process small amounts of magnetite may also appear (Fig. 8c2). The compositions of the pyrrhotite grains are presented in Appendix A.

(5) The group MD-oxPy (oxidized sulphides) was not observed in the thin sections and were identified only after rinsing and drying the magnetic residuum which suggests an artificial nature of this group. The separated particles are multimineral aggregates containing not only ferromagnetic phases but also silicates cemented by Fe-hydroxides (Fig. 8e).

4.1.2 Metavolcanics

(6) The group MV-Amf consists of phenocrysts of green amphiboles containing small intergrowths of magnetite/maghemite (Fig. 8f).

(7) The group MV-WR apart from dominant ferromagnetic phases such as magnetite and hematite also contains fine-grained silicate minerals (Fig. 8g). The ferromagnetic grain sizes are in the 10–20 μm range. The amount of magnetite prevails over hematite.

4.2 MicroMag magnetometer measurements

The results of the MicroMag experiments confirm that 4 groups of ferromagnetic grains separated from metadolerites are of low-coercivity where the IRM curves become saturated below 70–90 mT, $B_{cr} = 15$–30 mT (Table 2). Both groups of ferromagnetic grains separated from the metavolcanics revealed middle-high coercivity spectra which saturate in fields up to 340 mT, B_{cr} parameters—70–110 mT (Table 2).

The majority of samples are characterized by a magnetization ratio (M_r/M_s) of 0.1–0.3. The Coercivity ratio (B_{cr}/B_c) is more diverse and varies between 2 and 24. Most of the separates groups form evident clusters on the Day–Dunlop diagram. The majority of samples fall into pseudo-single-domain (PSD) sector of the plot (Dunlop 2002; Fig. 9). The metadolerite separates are located closer to the multidomain (MD) field than non-separated 'whole rock' samples of these rocks. The poor concentration of the metadolerites 'whole rock' samples on the Day–Dunlop diagram is related to the differences between major magnetic carriers in two locations where those rocks were sampled. Samples MD4 from Kinnefjellet are dominated by pyrrhotite in contrast to samples MD1-2 from St. Jonsfjorden which are dominated by magnetite. In the metadolerites the best correlation of the separates with the 'whole rock' samples are observed in the MD-Po-pyrrhotite and the MD-psMag titanite pseudomorphs after magnetite groups. These two groups are important sources of ferromagnetic signals in the metadolerites.

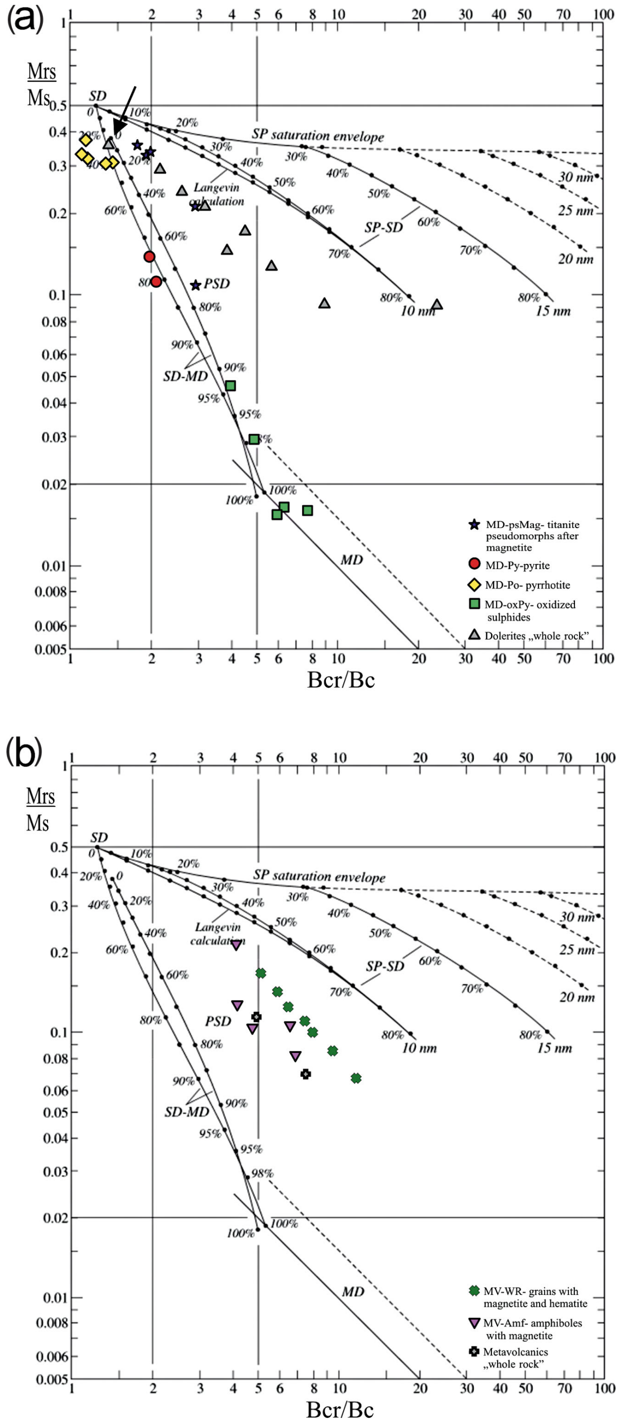

Figure 9. (a) Day–Dunlop plot for metadolerites, (b) Day–Dunlop plot for metavolcanics; both separates and non-separated samples were plotted on diagram (Dunlop 2002, mod.); SD, single domain; PSD, pseudosingle domain; SP, superparamagnetic; MD, multidomain. Results of ‘whole rock’ VSM experiment of MD4 pyrrhotite dominated sample is indicated by arrow.

MD-oxPy are distant from the sector occupied by ‘whole rock’ metadolerites samples which suggests they are not genetically related to the rest of magnetic carriers of investigated rock. It is suggested here that MD-oxPy group, which appeared during the process of separation of the samples, is the product of sulphide oxidation.

Both ‘whole rock’ and separate samples of the metavolcanics are well clustered in the same PSD area of the Day–Dunlop plot (Fig. 9). This suggests that the dominant magnetic carriers of metavolcanics are localized in analysed separates.

4.3 SIRM

The ferromagnetic separates exhibit the following unblocking temperatures:

4.3.1 Metadolerites

(1) Separates MD-psMag—the first heating curve reveals a maximum unblocking temperature around 575 °C corresponding to magnetite (Dunlop & Özdemir 1997; Fig. 10a).

(2) Separates MD-Py—as in the previous case the shape of thermal demagnetization diagram is characteristic for magnetite grains with unblocking temperature around 580 °C. An insignificant inflection of the first heating curve around 200 °C is also observed (Fig. 10b).

(3) Separates MD-Po—the SIRM diagram reveals a significant dominance of pyrrhotite which is demagnetized almost completely in the 320–330 °C range (Dekkers 1988; Dunlop & Özdemir 1997; Fig. 10c).

(4) Separates MD-oxPy—shows a decrease of the first heating curve intensity around 200 °C (Fig. 10d). The same diagram also reveals a small amount of magnetite/maghemite with a distinct temperature of 580 °C.

4.3.2 Metavolcanics

(5) Separates MV-WR—SIRM first heating curves reveal a maximum unblocking temperature around 680 °C (Fig. 10e) indicating the existence of hematite (Dunlop & Özdemir 1997). Notably, the first heating curves do not describe typical shapes for hematite grains, and are probably influenced by additional lower $T_{\mathrm{ub\ max}}$ ferromagnetic phases, possibly magnetite which was confirmed by optical/SEM identification. A significant inflection of the first heating SIRM curve is also observed around temperatures of 150–200 °C. The three-component IRM experiments (Lowrie 1990) conducted on ‘whole rock’ samples proved that this inflection is related to low-middle coercivity phases and excluded the influence of high coercivity goethite (Figs 6n and o).

(6) Separates MV-Amf—the diagram shows almost the same shape as the MV-WR separates with two unblocking temperatures around 150–200 and 575 °C (Fig. 10f) which are probably related to low $T_{\mathrm{ub\ max}}$ fine grained titanomagnetites/titanomaghemites and magnetite grains respectively (Dunlop & Özdemir 1997).

5 AGE OF FERROMAGNETIC CARRIERS

Petrographic and rock magnetic investigations presented in this contribution have revealed 6 main possible sources of ferromagnetic signals in the metabasites of Oscar II Land. In this section an attempt is made to correlate the identified ferromagnetic carriers with the palaeomagnetic record.

Detailed characteristics of the palaeomagnetic properties of the metabasites and possible tectonic and palaeogeographic interpretations of the palaeomagnetic results were presented in a sister paper (Michalski *et al.* 2017). In the presently investigated rocks

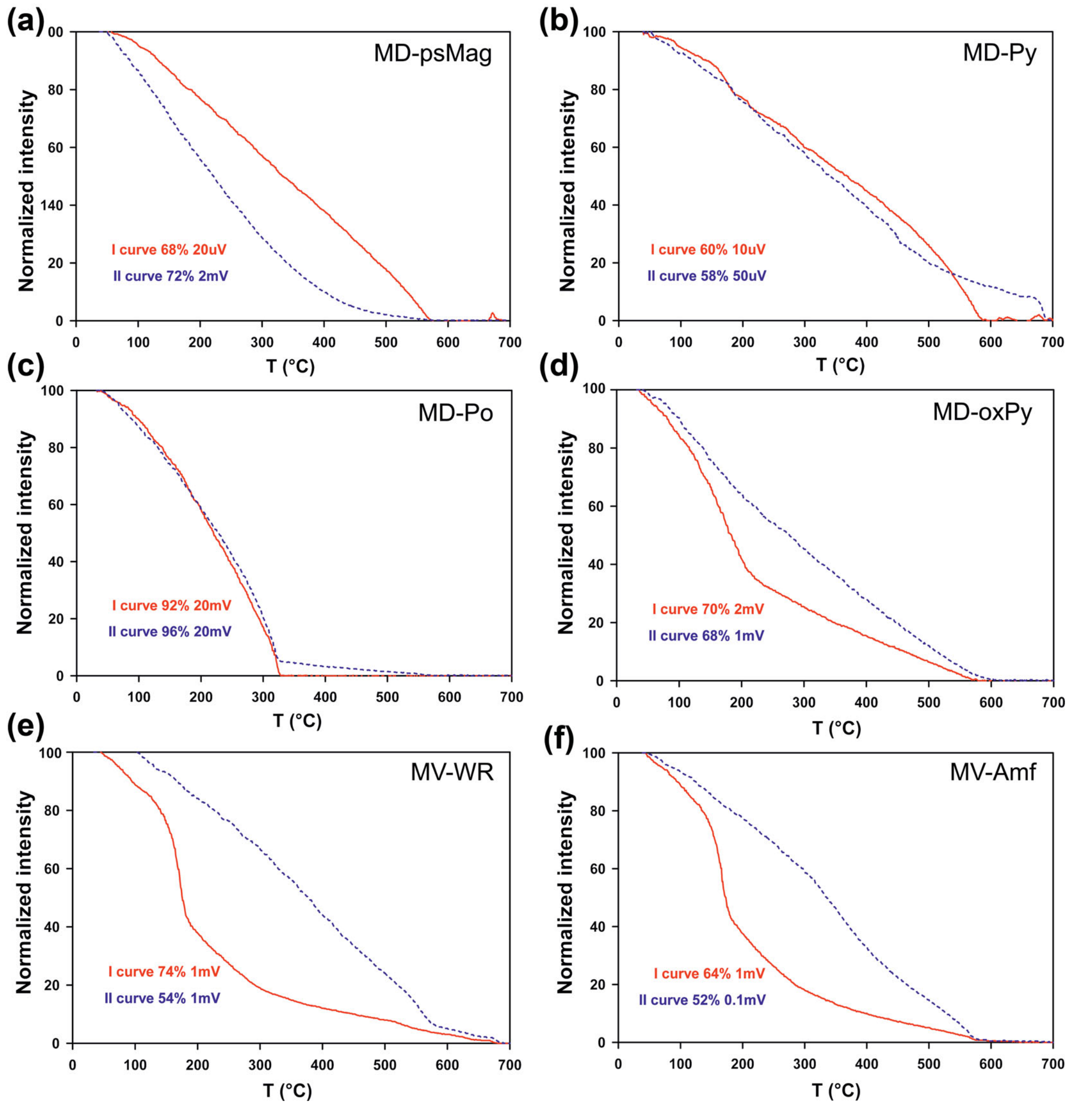

Figure 10. Saturation isothermal remanence magnetization (SIRM) curves for metadolerites (a–d) and metavolcanics (e,f) separates; curves were normalized to the maximum value of SIRM; experiments were conducted at room temperature; solid line: first heating curve, dashed line; second heating curve.

three main palaeomagnetic components characterized by different maximum unblocking temperatures ($T_{\mathrm{ub\,max}}$) were distinguished: L ($T_{\mathrm{ub\,max}} < 250\,^{\circ}$C), M ($250\,^{\circ}\mathrm{C} < T_{\mathrm{ub\,max}} < 350\,^{\circ}$C), H ($T_{\mathrm{ub\,max}} > 350\,^{\circ}$C), optionally MH ($T_{\mathrm{ub\,max}} > 250\,^{\circ}$C) by Michalski *et al.* (2017). The high inclinations of the L component are suggestive of a Mesozoic/Cenozoic age (Fig. 11; Michalski *et al.* 2017). The timing of the more stable M, H (MH) components is more ambiguous. Their inclination parameters indicate that they originated in low/moderate palaeolatitudes which suggests Upper Palaeozoic/Lower Mesozoic age (Fig. 11). On the other hand M, H (MH) VGPs do not fit Laurussia reference path (Fig. 12; Michalski *et al.* 2017), which suggests post-magnetization local/regional tectonic or palaeogeographic rotations. Those rotations are difficult to define given the complex tectonic evolution western Svalbard noted earlier and the controversial palaeogeographic position of Western Svalbard Terrane in Palaeozoic time and its proposed connections with Pearya (Trettin 1987; Harland 1997). In conclusion, it should be stressed that the applied *stricto* palaeomagnetic procedures in the metabasites accompanied by *in situ* LA-ICP-MS 40Ar/39Ar age determinations in adjacent rocks (Michalski *et al.* 2017), suggest important thermal remagnetizations during the 426–380 Ma Caledonian (*sensu lato*) metamorphism, the 377–326 Ma and *c.* 300 Ma intervals and the substantial influence of the regional tectonic rotations on the observed palaeomagnetic record which includes listric fault generated rotations related to the North Atlantic extensional tectonism. They do not exclude, however, the preservation of any pre-Caledonian (Proterozoic/Lower Palaeozoic) or primary ferromagnetic carriers in the investigated rocks.

The investigations presented in this contribution confirm the abundance of pyrrhotite and magnetite as the principal carriers that were generated during the Caledonian metamorphism of the metadolerites. The spatial relations of the identified ferromagnetic minerals to other rock-forming minerals in MD-Py, MD-Po leave no doubt that they originated in metamorphic environment. Two other groups of grains, MD-Ilm and MD-Py, were carefully examined to determine whether they contained any relicts of older pre-Caledonian carriers in metadolerites:

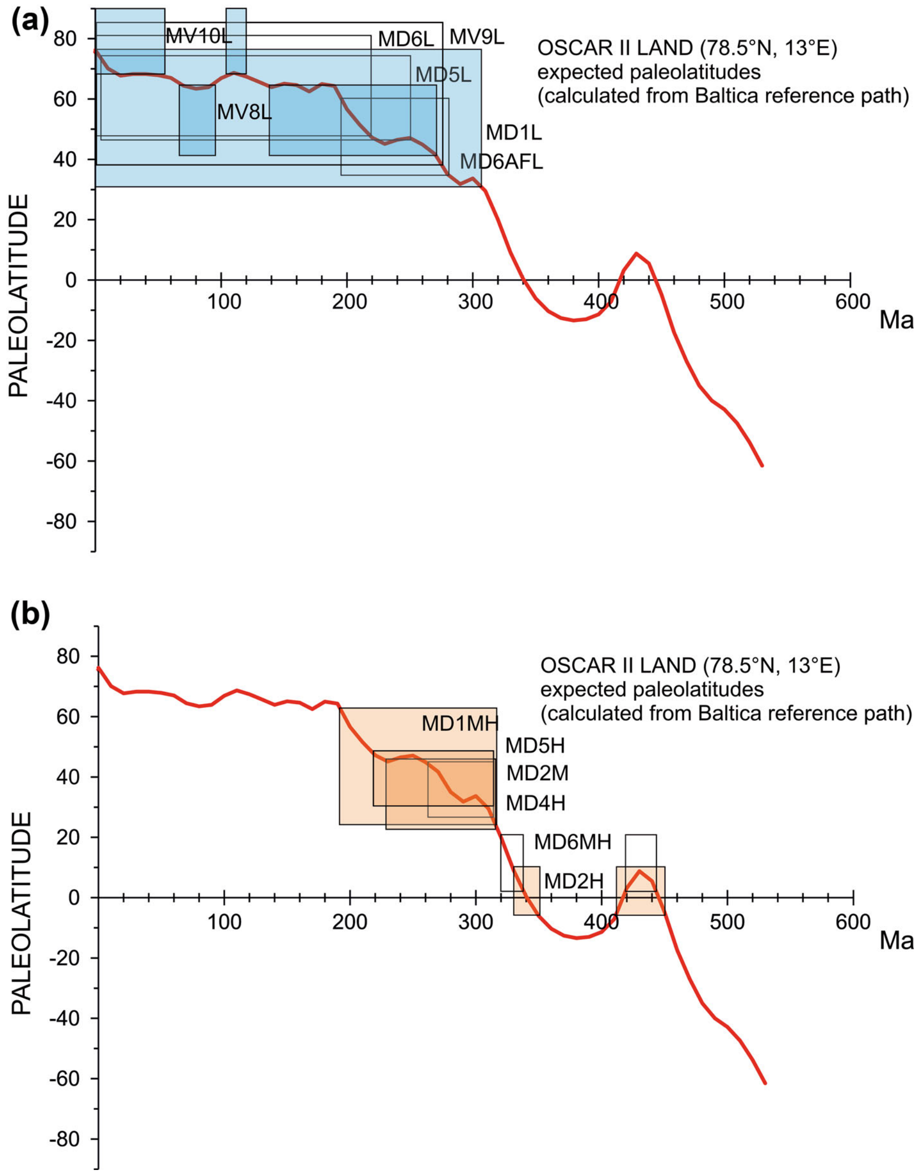

Figure 11. Palaeolatitudes of the Western Terrane of Svalbard during magnetization of palaeomagnetic directions identified in metabasites of Oscar II Land against palaeolatitudes expected in Phanerozic for Oscar II Land; (a) palaeolatitudes calculated from low coercivity/$T_{\mathrm{ub\ max}}$ components, (b) from middle/high $T_{\mathrm{ub\ max}}$ components; MD, metadolerites sites; MV, metavolcanics sites; palaeolatitude curve for Oscar II Land sampling area (78.5 °N, 13 °E) has been calculated from Baltica APWP, derived from GMAP 2012 palaeopoles libraries; all palaeolatitudes of Oscar II Land metabasites are recalculated for northern hemisphere and are presented with confidence limits defined by D_p (half-axis of palaeopole oval of the confidence limit $\alpha95$); highlighted are components from sites which were subjected to mineral separation (this study).

(1) MD-Ilm, represented by ilmenite phenocrysts containing visible voids after dissolution of hematite intergrowths were initially proposed as one of the ferromagnetic carriers in the metadolerites. The applied high resolution petrographic and rock magnetic methods did not confirm the presence of any hematite remnants. The lack of the hematite intergrowths confirmed in several separate grains by MicroMag experiments, indicates that metamorphic alteration of the oxides in the metadolerites was complete.

(2) MD-psMag is represented by the titanite pseudomorphs after primary/magmatic magnetite. The rock magnetic experiments (Micromag, SIRM) confirmed the presence of magnetite in these grains. The magnetite in these pseudomorphs may represent remnants of the primary Ti-bearing magnetite that did not breakdown into titanite, or that may have crystallized contemporaneously with titanite during greenschist metamorphism. Low-Ti magnetite is a common product of the metamorphic breakdown of the titanomagnetite (e.g. Frost & Lindsley 1991; Shau *et al.* 2000).

It can be concluded from the above that in the metadolerites the only possible source of pre-Caledonian signal would be from relicts of primary magnetites in titanite pseudomorphs. Taking into account the character of the metadolerites textures and the intensity of metamorphic processes observed in ilmenites (MD-Ilm), a pre-metamorphic origin of MD-psMag magnetites is unlikely.

The separation of the Fe-containing grains in the metavolcanics did not result in the isolation of genetically different types of ferromagnetic carriers. Both types of separated grains MV-Amf, MV-WR

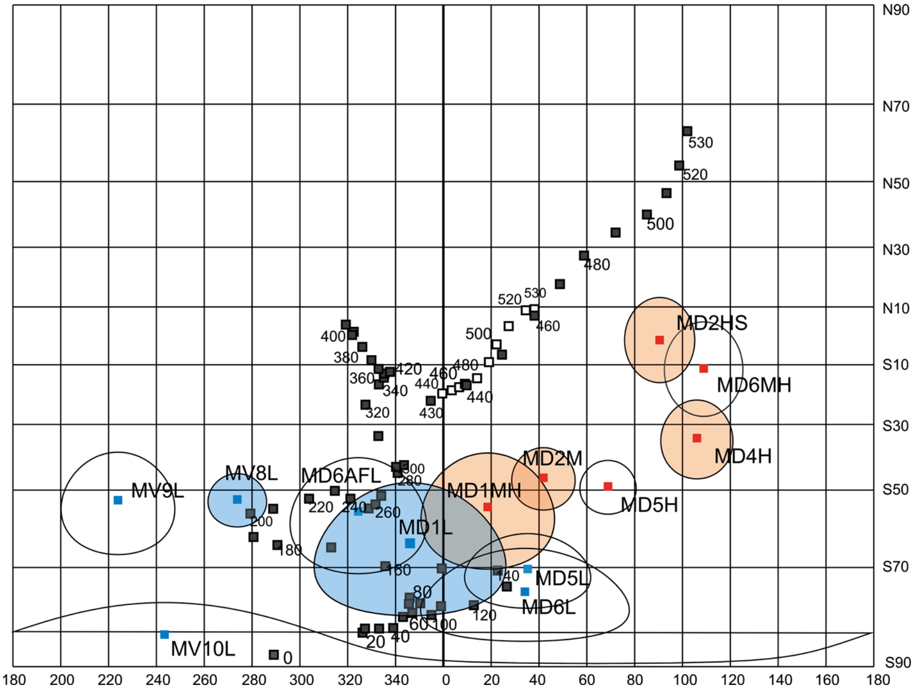

Figure 12. Palaeopoles calculated from palaeomagnetic directions identified in OIIL metabasites with their ellipses of the confidence limit $\alpha 95$ against reference path of Laurussia (palaeopoles 0–430 Ma, closed squares), Baltica (palaeopoles 0–430 Ma, closed squares), Baltica (palaeopoles 440–530 Ma, closed squares) and Laurentia (palaeopoles 440–530 Ma, open squares); reference palaeopoles were taken from Torsvik *et al*. (2012), ages of particular reference palaeopoles are given; MD, metadolerites sites; MV, metavolcanics sites; highlighted are VGPs from the sites which were subjected to mineral separation; blue symbols, low coercivity/$T_{\mathrm{ub\,max}}$ components palaeopoles; red symbols, middle-high $T_{\mathrm{ub\,max}}$ components; Galls projection.

are multi-mineral aggregates containing magnetite and hematite. The observed textural and other petrological features suggest that the MV-Amf, MV-WR groups could be related, respectively, to magmatic and/or syn/post-metamorphic stages. It should be noted, however, that in case of the metavolcanics, the question of the preservation of pre-Caledonian magnetization is less important. The NRM structure is dominated by the low temperature component L ($T_{\mathrm{ub\,max}} < 250\,^{\circ}$C) which constitutes up to 60–70 per cent of NRM signal (Michalski *et al*. 2017). Its high inclination is suggestive of a Mesozoic/Cenozoic re-magnetization overprint (Figs 11 and 12). The instability of the metavolcanic samples above 250 °C prevented the identification of any other (older?) palaeomagnetic directions.

6 CONCLUSIONS

(1) The Integrated 'whole rock' versus 'Fe-containing separates' petrographic–rock magnetic experiments have improved the detailed identification of ferromagnetic phases in the investigated metabasites and constrained their origin:

(i) the metadolerites contain magnetite intergrowths in titanites, magnetites in parageneses with metamorphic minerals (e.g. sulphides) and pyrrhotites,

(ii) the metavolcanics contain magnetites and hematites in the majority metamorphic assemblages and low-coercivity minerals, possibly fine-grained titanomagnetite/titanomaghemite, that were demagnetized at temperatures around 150–200 °C.

(2) The results of our investigations strongly suggest that all of ferromagnetic mineral phases related to pre-metamorphic stages of the investigated metadolerites were broken down or recrystallized. Rock magnetic experiments of separated grains of ilmenites confirmed a complete dissolution of the ferromagnetic intergrowths of hematite during the Caledonian metamorphism. The weak magnetite signal recorded in the separated titanite grains is probably related to fine magnetite and/or maghemite that had grown contemporaneously with metamorphic pyrite and/or titanite.

(3) The results of the experiments conducted on the metavolcanics has allowed the precise location of the ferromagnetic signal within investigated rocks. However, in this case, based on the applied methods, the existence of the ferromagnetic pre-Caledonian relicts cannot be excluded.

(4) The applied method of separation significantly improved the process of ferromagnetic mineral identification. It was possible to define the sources of ferromagnetic signal, place them in a textural context and relate them to particular stages of investigated rock history. In many cases the process of separation provided a unique opportunity to conduct 'rock magnetic' experiments on natural 'mono-mineral' samples or 'Fe-containing aggregates' formed during a single tectono-thermal evolution stage. The derived new data related to origin of the ferromagnetic carriers has significantly improved the interpretation of palaeomagnetic directions.

ACKNOWLEDGEMENTS

This study is part of PALMAG project (2012-2016): 'Integration of palaeomagnetic, isotopic and structural data to understand Svalbard Caledonian Terranes assemblage' funded by Polish National Science Centre (NSC)—grant number 2011/03/D/ST10/05193. Material for investigations described in this paper was collected in the course of PALMAG project from the southwestern area of Oscar II Land (Western Spitsbergen). The publication is also partially financed from the funds of the Leading National Research Centre (KNOW) received by the Centre for Polar Studies for the period 2014–2018 and partially supported within statutory activities No.

3841/E-41/S/2015 of the Ministry of Science and Higher Education of Poland. We are very grateful to the reviewers and editors for their comments and suggestions to the original manuscript. We would also like to thank to A. Hołda-Michalska for preparation of maps and improvements of figures.

REFERENCES

Clark, S.A., Glorstad-Clark, E., Faleide, J.I., Schmid, D., Hartz, E.H. & Fjeldskaar, W., 2014. Southwest Barents Sea rift basin evolution: comparing results from backstripping and time forward modelling, *Basin Res.,* **26,** 550–566.

Dallmeyer, R.D., 1989. Partial thermal resetting of ^{40}Ar/^{39}Ar mineral ages in western Spitsbergen, Svalbard: possible evidence for Tertiary metamorphism, *Geol. Mag.,* **126,** 587–593.

Dalstra, H. & Guedes, S., 2004. Giant hydrothermal hematite deposits with Fe-Mg metasomatism: a comparison of the Carajás, Hamersley, and other iron ores, *Econ. Geol.,* **99,** 1793–1800.

Dekkers, M.J., 1988. Magnetic proprties of natural pyrrhotite: Part 1: Behawior of initial susceptibility and saturation-magnetization related parameters in a grain-size dependent framework, *Phys. Earth planet. Inter.,* **52,** 376–393.

Dunlop, D.J., 2002. Theory and application of the Day plot (M_{rs}/M_s versus H_{cr}/H_c): 1. Theoretical curves and tests using titanomagnetite data, *J. geophys. Res.,* **107,** EPM 4-1–EPM 4-22.

Dunlop, D.J. & Özdemir, Ö., 1997. *Rock Magnetism Fundamentals and Frontiers,* Cambridge Univ. Press, pp. 596.

Dunlop, D.J., Özdemir, Ö. & Rancourt, D.G., 2006. Magnetism of biotite crystals, *Earth planet. Sci. Lett.,* **243,** 805–819.

Dunlop, D.J., Zhang, B. & Özdemir, Ö., 2005. Linear and nonlinear Thellier paleointensity behaviour of natural minerals, *J. geophys. Res.,* **110,** B01103, doi:10.1029/2004JB003095.

Frost, B.R. & Lindsley, D.H., 1991. Occurrence of iron-titanium oxides in igneous rocks, *Rev. Mineral.,* **25,** 469–487.

Gasser, D. & Andresen, A., 2013. Caledonian terrane amalgamation of Svalbard: detrital zircon provenance of Mesoproterozoic to Carboniferous strata from Oscar II Land, western Spitsbergen, *Geol. Mag.,* **150,** 1103–1126.

Haggerty, S.E., 1991. Oxide textures—A mini-atlas, *Rev. Mineral.,* **25,** 129–219.

Harland, W.B., 1997. The geology of Svalbard, *Geol. Soc. Lond.*, *Memoir* 17, pp. 521.

Harland, W.B. & Wright, N.J.R., 1979. Alternative hypothesis for the pre-Carboniferous evolution of Svalbard, *Norsk Polarinst Skri,* **167,** 89–117.

Harlov, D., Tropper, P., Seifert, W., Nijland, T. & Förster, H.J., 2006. Formation of Al-rich titanite ($CaTiSiO_4O$–$CaAlSiO_4OH$) reaction rims on ilmenite in metamorphic rocks as a function of fH_2O and fO_2, *Lithos,* **88,** 72–84.

Hjelle, A., Piepjohn, K., Saalmann, K., Ohta, Y., Salvigsen, O., Thiedig, F. & Dallmann, W., 1999. Geological map of Svalbard 1:100 000, sheet A7G Kongsfiorden, *Norsk Polarinst* Temakart No. 30.

Hurai, V. & Huraiová, M., 2011. Origin of ferroan alabandite and manganoan sphalerite from the Tisovec skarn, Slovakia, *N. Jb. Miner. Abh.,* **188,** 119–134.

Kądziałko-Hofmokl, M., 2001. Rock-magnetic study of Gogołów-Jordanów serpentinite unit of the Paleozoic Sudetic ophiolite (South Poland), *Ofiolit* **26**(2B), 425–432.

Kądziałko-Hofmokl, M. & Kruczyk, J., 1976. Complete and partial self-reversal of natural remanent magnetization of basaltic rocks from Lower Silesia, Poland, *Pure appl. Geophys.,* **114**(2), 207–213.

Lowrie, W., 1990. Identification of ferromagnetic minerals in a rock by coercivity and unblocking temperature properties, *Geophys. Res. Lett.,* **17,** 159–162.

Maloof, A.C., Halverson, G.P., Kirschvink, J.L., Schrag, D.P., Weiss, B.P. & Hoffman, P.F., 2006. Combined paleomagnetic, isotopic, and stratigraphic evidence for true polar wander from the Neoproterozoic Akademikerbreen Group, Svalbard, Norway, *Geol. Soc. Am. Bull.,* **118,** 1099–1124.

Matzka, J. & Krása, D., 2007. Oceanic basalt continuous thermal demagnetization curves, *Geophys. J. Int.,* **169,** 941–950.

Michalski, K., Lewandowski, M. & Manby, G.M., 2012. New palaeomagnetic, petrographic and ^{40}Ar/^{39}Ar data to test palaeogeographic reconstructions of Caledonide Svalbard, *Geol. Mag.,* **149,** 696–721.

Michalski, K., Nejbert, K., Domańska-Siuda, J. & Manby, G., 2014. New palaeomagnetic data from metamorphosed carbonates of Western Spitsbergen, Oscar II Land, *Pol. Polar Res.,* **35,** 553–592.

Michalski, K., Manby, G., Nejbert, K., Domańska-Siuda, J. & Burzyński, M., 2017. Using palaeomagnetic and isotopic data to investigate late to post-Caledonian tectonothermal processes within the Western Terrane of Svalbard, *J. Geol. Soc. Lond.,* doi:10.1144/jgs2016-037.

Ohta, Y., 1985. Geochemistry of Precambrian igneous rocks between St. Jonsfjorden and Isfjorden, central Western Spitsbergen, Svalbard, *Polar Res.,* **3,** 49–67.

Özdemir, Ö., 1987. Inversion of titanomaghemites, *Phys. Earth planet. Inter.,* **46,** 184–196.

Ramdohr, P., 1980. *The Ore Minerals and their Intergrowths,* Pergamon Press.

Shau, Y.H., Torii, M., Horng, C.S. & Peacor, D.R., 2000. Subsolidus evolution and alteration of titanomagnetite in ocean ridge basalts from Deep Sea Drilling Project/Ocean Drilling Program Hole 504B, Leg 83: implications for the timing of magnetization, *J. geophys. Res.,* **105**(B10), 635–649.

Tessensohn, F., Von Gosen, W. & Piepjohn, K., 2001. Permo-carboniferous slivers infolded in the basement of Western Oscar II Land, in *Intra-Continental Fold Belts, CASE 1*: Western Spitsbergen. *Geologisches Jahrbuch B91*, pp. 161–199, ed. Tessensohn, F., Schweizerbart Science Publishers.

Torsvik, T.H. *et al.*, 2012. Phanerozoic polar wander, paleogeography and dynamics, *Earth-Sci. Rev.,* **114,** 325–368.

Trettin, H.P., 1987. Pearya: a composite terrane with Caledonian affinities in northern Ellesmere Island, *Can. J. Earth Sci.,* **24,** 224–245.

Xirouchakis, D. & Lindsley, D.H., 1998. Equilibria among titanite, hedenbergite, fayalite, quartz, ilmenite and magnetite: experiments and internally consistent thermodynamic data for titanite, *Am. Mineral.,* **83,** 712–725.

SUPPORTING INFORMATION

Supplementary data are available at *GJI* online.

Appendix A

Table App. A1. Chemical composition of the magnetite occurred as fine intergrowths within pyrite *(*MD-Py). Analyses were taken in the pyrite aggregate illustrated in Fig. 8(b).

Table App. A2. Chemical composition of the ilmenite (Ilm-1) recognized as relics of primary magmatic phases. Analysed ilmenite grains are illustrated in Fig. 8(a).

Table App. A3. Chemical composition of pyrite (MD-Py). Analysed grains are illustrated in Fig. 8(b).

Table App. A4. Chemical composition of pyrrhotite (MD-Po). Analysed grains are illustrated in Figs 8(c1) and (c2).

Appendix B

Figure App. B1. Petrography of metadolerites. (A) Well preserved igneous texture defined by albite pseudomorph after plagioclase and clinopyroxene, both euhedral. Sample MD2. (B) Unalterd euhedral clinopyroxene within albite matrix. The black aggregates consist of recrystallized Fe-Ti oxides, rimmed by biotite aggregates. Sample MD1. (C) Metadolerite with relict igneous clinopyroxene, kaersutite, apatite and biotite and metamorphic actinolite, albite and chlorite. Sample MD1. (D) Metadolerite showing penetrative S1 syn-metamorphic foliation. Many pre- to early S1 opaque phases show varying degrees of rotation and pressure shadows.

Abbreviations: Cpx, clinopyroxene; Krs, kaersutite; Ap, apatite; Bt, biotite; Act, actinolite; Ab, albite; Chl, chlorite.

Figure App. B2. Petrography of metavolcanic rocks. (A) Fine-grained metavolcanic rocks, with visible albite pseudomorphs after plagioclase, and irregular calcite veinlets. Sample MV8. (B) Calcite and chlorite aggregates mark weak foliation within metavolcanic rocks. The black aggregates are highly altered Fe-Ti oxide phenocrysts (magnetite and ilmenite). Sample MV8. (C) Metavolcanic rocks with porphyritic texture, containing relics of plagioclase and amphibole phenocrysts and calcite veins. Sample MV10. (D) Albite and chlorite pseudomorph after igneous plagioclase and clinopyroxene. Sample MV10. Abbreviations: Ab, albite; Amp, amphibole; Bt, biotite; Cc, carbonate; Chl, chlorite.

Figure App. B3. Mineralogy of Fe-Ti oxides in metadolerites. (A) Unalterd ilmenite phenocrysts and titanite-siderite-pyrrhotite pseudomorph after Ti-bearing magnetite. Sample MD1. (B) Texture showing breakdown of ilmenite into titanite. Sample MD2. (C) Ilmenite phenocrysts with minute intergrowths of titanite. Sample MD1. (D) Pseudomorph after magnetite (psMag) associated with pyrite and ilmenite. Sample MD1. Abbreviations: Ilm, ilmenite; Po, pyrrhotite; Py, pyrite; Ttn, titanite; psMag, titanite/siderite pseudomorph after Ti-bearing magnetite.

Figure App. B4. Mineralogy of sulphides in metadolerite. (A) Pyrrhotite grain with fine exsolution of pentlandite, replaced by goethite at the contact with silicates. In addition, igneous ilmenite surrounded by a metamorphic titanite, developed during metamorphism of greenschist facies conditions. Sample MD2. (B) Breakdown of ilmenite into titanite. Pyrite aggregates may contain minute intergrowths of pyrrhotite and magnetite. Sample MD1. (C) Secondary aggregate after igneous magnetite, composed of ilmenite, titanite, siderite, pyrite and pyrrhotite. Sample MD1. (D) Pyrrhotite-chalcopyrite aggregate, partially replaced by marcasite. Sample MD4. Abbreviations: Ccp, chalcopyrite; Gth, goethite; Ilm, ilmenite; Mr, marcasite; Pn, pentlandite; Po, pyrrhotite; Py, pyrite; Ttn, titanite; psMag, pseudomorph after magnetite.

Figure App. B5. Mineralogy of Fe-Ti oxides in metavolcanic rocks. (A,B) Small euhedral magnetite and hematite grains dispersed within matrix (albite+chlorite) of metavolcanic rocks. Sample MV8. (C) Altered phenocryst of magnetite and ilmenite that have been replaced by titanite and then overgrown with hematite. Sample MV10. (D) Texture of hematite—titanite–albite pseudomorph after igneous ilmenite. Sample MV10. Abbreviations: Hm, hematite; Mag, magnetite; Ttn, titanite; psIlm, titanite-albite pseudomorph after ilmenite.

Figure App. B6. Mineralogy of sulphides in metavolcanic rocks. Sulphides in this rock are present as accessory minerals. (A) Chalcopyrite–hematite association. Dispersed small euhedral magnetite and hematite grains occur in the matrix. Sample MV8. (B) Large pyrrhotite grain replaced by goethite. Sample MV8. Abbreviations: Ccp, chalcopyrite; Gth, goethite; Hm, hematite; Mgt, magnetite; Po, pyrrhotite.

Please note: Oxford University Press is not responsible for the conten or functionality of any supporting materials supplied by the authors. Any queries (other than missing material) should be directed to the corresponding author for the paper.